Journal Pre-proof

A fast-running engineering tool for assessing structural vulnerability to blast loading

Carlo Crispino, Salvatore Annunziata, Alberto Contini, Luca Lomazzi, Andrea Manes

PII: S2214-9147(24)00283-6

DOI: https://doi.org/10.1016/j.dt.2024.12.009

Reference: DT 1548

To appear in: *Defence Technology*

Received Date: 19 September 2024

Revised Date: 21 November 2024

Accepted Date: 9 December 2024

Please cite this article as: Crispino C, Annunziata S, Contini A, Lomazzi L, Manes A, A fast-running engineering tool for assessing structural vulnerability to blast loading, *Defence Technology*, https://doi.org/10.1016/j.dt.2024.12.009.

A fast-running engineering tool for assessing structural vulnerability to blast loading

Carlo Crispino [a], Salvatore Annunziata [a, *], Alberto Contini [a], Luca Lomazzi [a] and Andrea Manes [a]

[a] Politecnico di Milano, Department of Mechanical Engineering, Via Giuseppe La Masa, 1, Milan 20156, Italy

***Corresponding author:** Salvatore Annunziata
E-mail: salvatore.annunziata@polimi.it

A fast-running engineering tool for assessing structural vulnerability to blast loading

Abstract

Assessing the vulnerability of a platform is crucial in its design. In fact, the results obtained from vulnerability analyses provide valuable information, leading to precise design choices or corrective solutions that enhance the platform's chances of surviving different scenarios. Such scenarios can involve various types of threats that can affect the platform's survivability. Among such, blast waves impacting the platform's structure represent critical conditions that have not yet been studied in detail. That is, frameworks for vulnerability assessment that can deal with blast loading have not been presented yet. In this context, this work presents a fast-running engineering tool that can quantify the risk that a structure fails when it is subjected to blast loading from the detonation of high explosive-driven threats detonating at various distances from the structure itself. The tool has been implemented in an in-house software that calculates vulnerability to various impacting objects, and its capabilities have been shown through a simplified, yet realistic, case study. The novelty of this research lies in the development of an integrated computational environment capable of calculating the platform's vulnerability to blast waves, without the need for running expensive finite element simulations. In fact, the proposed tool is fully based on analytical models integrated with a probabilistic approach for vulnerability calculation.

Keywords: Vulnerability; Blast loading; Probabilistic assessment; Analytical models; Fast-running engineering tool

1. Introduction

Aircraft survivability refers to a platform's capacity to evade or endure hostile conditions created by humans, while killability, or kill probability, quantifies the likelihood of the platform being destroyed when encountering a threat [1].

Survivability evaluation has been applied to aerial, naval, and terrestrial platforms with the aim of identifying criticalities and eventually driving corrective actions. Such corrective actions can be considered both in the design phase and after the platform has been built up. In the former case, for example, the position of the platform's components can be modified so as to lower the identified vulnerabilities. In the latter case, instead, protective components can be designed so to reduce the kill probability and make the chances of concluding the assigned mission higher [2].

The discipline of survivability originated in the early days of the 20th century [3], and was further developed during World War I from the main necessity of protecting the platform's occupants from threats. Pilots in that era adopted two primary tactics to enhance survivability: flying above the maximum altitude of enemy weapons and using stove lids as protective shields against potential threats. The former tactic addresses susceptibility, defined as the aircraft's inability to evade the components of an enemy's defense constituting the hostile environment. Instead, the latter tactic addresses vulnerability, defined as the aircraft's inability to survive the encounter with a threat.

Significant advancements in the combat survivability discipline date back to the '80s, when the concepts of survivability and vulnerability were first formalized [1]. Moreover, in 1984, the Survivability/Vulnerability Information Analysis Center (SURVIAC) was established, with the objective of providing technical support in non-nuclear survivability [4]. The decision to improve aircraft's survivability taken in the '80s resulted in 1991 in 1800 successful strikes at night by F-117s, during Operation Desert Storm (Gulf War), as a result of the combination of stealth and electronic attack capabilities [5]. More recently, the JSF program, which began between the '80s and '90s and culminated in the development of the F35 aircraft, was the first case in which survivability assessment was emphasized during the design process [1, 2]. This fighter aircraft, together with the F22, was characterized by survival probability approaching 100% when considering the enemy's threats against which the jet was designed [6].

So far, studies on survivability have been mainly focused on ballistic threats. Among the many contributions, a study published in 1986 about single-hit vulnerability assessment is worth mentioning [7]. Survivability analyses typically adopt a statistical approach, requiring a substantial amount of data. The advancement in calculating capacity and the development of dedicated software packages, such as FASTGEN and COVART [8–10], have facilitated this process. These advancements allowed the introduction of direct simulation methods to assess the multi-hit vulnerability of aircraft with overlapping components, such as in Ref. [11], which is based on the statistical framework of the Monte Carlo method proposed in Ref. [12].

Research has also been conducted on threats posed by missiles equipped with fragmentation warheads. A simplified, yet comprehensive, approach for assessing the vulnerability of military aircraft to multiple-hit scenarios involving fragmentation warheads was outlined in Ref. [13]. This approach involved analyzing various aspects, such as the dispersion of missile fragments to determine hit locations, the penetration of fragments into target components, and ultimately estimating the overall likelihood of the aircraft being disabled using a fault tree analysis. Additionally, a criterion for assessing the potential explosion of fuel tanks was incorporated to evaluate platform vulnerability. Subsequently, in Ref. [14], the framework was further refined by introducing the concept of the mean volume of the effectiveness of the warhead. However, the work did not address damage caused by the blast wave resulting from the detonation of the high explosive material contained within the missile core.

Damage from blast wave has been addressed more recently in Ref. [15], which expanded upon the initial investigation of the blast event proposed in Ref. [1]. This refinement allowed for determining the platform's kill state by modeling and assessing the structural vibration of aircraft components within an elastoplastic framework. A maximum allowable displacement criterion was considered to assess the probability of the target being disabled due to blast loads. To the authors' best knowledge, no other publicly available studies have been presented concerning blast loading of aerial structures yet, while extensive literature can be found for other fields, such as for buildings and civil vehicles [16]. Additionally, structural damage induced by blast waves is assessed most of the time by finite element simulations, which are expensive and cannot be considered for platform design [17].

In this context, this work presents a vulnerability-driven approach that leverages state-of-the-art methods for analyzing blast-loaded aeronautical structures, particularly wings. The proposed approach consists of an analytical model integrated into in-house software for vulnerability assessment, which was previously developed considering other types of threats, such as projectiles and fragments. The updated environment aims to efficiently assess structural vulnerability under blast loads, relying on simplified analytical approaches to avoid the computational cost of finite element simulations.

This paper is organized as follows. Section 2 is dedicated to the description of the approach and the software package. Section 3 presents a case study to test the proposed approach against a wing of a Northrop Grumman RQ-4A Global Hawk. The case study also demonstrated the proposed framework by conducting a full vulnerability assessment of the wing and some platform's components to both multi-hits and missile threats. Finally, the conclusions of the work are drawn out in Section 4.

2. Methods

Comprehensively assessing the vulnerability of blast-loaded structures requires evaluating the structural response when the detonation occurs at several points in space, so as to study the structure's weak points from different directions. Then, the information gained at all detonation points needs to be combined into a single probabilistic indicator that defines the vulnerability of the structure. According to this approach, many simulations need to be carried out to thoroughly evaluate the structure under consideration. Consequently, this Section presents an efficient and fast-running computational method for assessing the vulnerability of blast-loaded structures, focusing on aeronautical structures.

The method employs an analytical module for evaluating the pressure load, a two-step geometrical modeling of the structure, and finally a module for the evaluation of the structural dynamic response. In regard to the geometrical modeling, first, the structure and its constraints are modeled as an equivalent beam with appropriate boundary conditions. Then, such a beam is modeled as a single-degree-of-freedom system (SDOF method) to study its dynamic response under blast loading. A criterion based on the maximum deflection of the equivalent system is considered to define when the structure becomes inoperative. Such inoperative condition also requires computing an allowable limit for the structural deflection, which is estimated by calculating the plastic limit of the equivalent beam, assuming that the structure cannot work anymore after the moment capacity at the supports reaches a defined threshold due to the blast load.

The proposed methodology is demonstrated below by considering the wing of a representative aeronautical platform. Two main assumptions have been made: (i) the equivalent beam representation of the wing is assumed to be a cantilever beam, and (ii) the structure is no longer operative when plastic hinges start to appear at the clamp.

2.1. Load evaluation

The pressure load generated by the blast is analytically modeled through the *TNT equivalent* method, which allows predicting the load based on the scaled distance $Z = R \cdot W^{-1/3}$, where R is the distance from the center of the detonation and W the TNT equivalent weight of the explosive charge [16–18]. Upon impact, the incident blast waves generate a reflected blast wave, with a more critical pressure-time history. This behavior is shown in Fig. 1, where P_r indicates the reflected overpressure, P_s the incident overpressure, and t_{pos} the positive phase duration of the load. In the figure, the pressure-time history concerning the blast wave that interacts perpendicularly with the front face of a structure is depicted. However, this behavior is qualitatively valid also for waves that impact the structure with a different incidence angle. Quantitatively, the theory is extended by computing the new reflected overpressure P_r by means of Eq. (1).

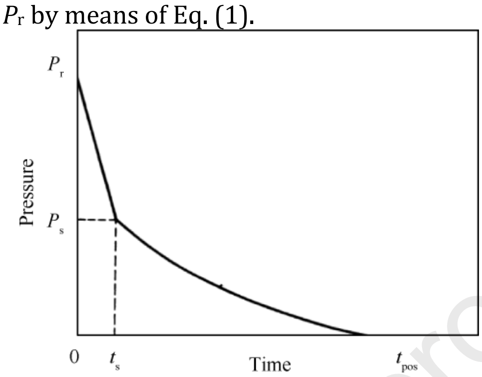

Fig. 1. Representative pressure-time history of the blast load on a structure. Reprint from Ref. [19].

$$P_r = c_{r\alpha} P_s \tag{1}$$

where $c_{r\alpha}$ is the reflected pressure coefficient, which depends on the incidence angle α and is obtained by fitting to experimental curves [20]. The incident overpressure value P_s is evaluated through Eq. (2) [21]

$$P_s = \frac{808 \cdot P_0 \cdot \left[1 + \left(\frac{Z}{4.5}\right)^2\right]}{\sqrt{\left[1 + \left(\frac{Z}{0.048}\right)^2\right]} \cdot \sqrt{\left[1 + \left(\frac{Z}{0.32}\right)^2\right]} \cdot \sqrt{\left[1 + \left(\frac{Z}{1.35}\right)^2\right]}} \tag{2}$$

where P_0 is the ambient pressure. Finally, the positive phase duration t_{pos} can be evaluated through Eq. (3)

$$t_{pos} = \frac{980 \cdot \sqrt[3]{W} \cdot \left[1 + \left(\frac{Z}{0.54}\right)^{10}\right]}{\left(1 + \left(\frac{Z}{0.02}\right)^3\right) \cdot \left(1 + \left(\frac{Z}{0.74}\right)^6\right) \cdot \sqrt{1 + \left(\frac{Z}{6.9}\right)^2}} \tag{3}$$

2.2. Geometrical modeling

The geometrical modeling module is used to define a simplified structure that is dynamically equivalent to the structure under assessment. In the interest of clarity, the case of a beam as the dynamic equivalent of an aeronautical wing is described here. The simplification requires evaluating the wing total mass M_{tot} and moment of inertia J_{tot}.

Based on typical solutions adopted in aeronautical platform design, the wing structure is supposed to be made of (i) a single spar with a hollow rectangular cross-section, (ii) the skin, and (iii) several ribs. The former two elements contribute to both the mass and the equivalent moment of inertia of the wing, while the ribs, due to their low thickness, provide no resistance to longitudinal deflection, and their presence is accounted for only in terms of mass. Exploiting the additive property of the moment of inertia, J_{tot} is evaluated by summing up the moments of inertia of the spar and the skin. While the geometrical properties of the spar are straightforward to calculate given its hollow rectangular shape, a numerical approach has been developed for the skin: the approach takes in the NACA codification string, which provides information about the airfoil shape, then the skin cross-section is discretized into small rectangular elements (Fig. 2), and the value of the moment of inertia of each element is calculated with respect to its local neutral axis. The global neutral axis of the skin is inclined with respect to the local neutral axis of each element, and it is located at a certain distance from it. Eqs. (4) and (5), namely, the transformation equation and the parallel axis theorem are then employed

$$J_{\mathrm{loc},i} = J_{xi,\mathrm{loc}}\cos\left(\theta_i\right)^2 + J_{yi,\mathrm{loc}}\sin\left(\theta_i\right)^2 \; J_{\mathrm{skin}} = \sum_{i=1}^{N_{el}}\left(J_{\mathrm{loc},i} + area_i \cdot d_i^2\right) \quad (4)$$

$$J_{\mathrm{skin}} = \sum_{i=1}^{N_{el}}\left(J_{\mathrm{loc},i} + area_i \cdot d_i^2\right) \quad (5)$$

where θ_i is the inclination angle between the local neutral axis of the i-th rectangular element and the global neutral axis of the skin, and d_i is the distance between them. $J_{\mathrm{loc},\,i}$ is the local moment of inertia of the i-th element without considering the parallel axis contribution. The NACA codification is also exploited to calculate the cross-sectional area of the ribs through Eq. (6) [22]

$$A_{rib} = \int_0^c \left(2 \cdot y_t(x)\right) \mathrm{d}x \quad (6)$$

where $y_t(x)$ is the thickness function, which provides the coordinates of the airfoil profile, as shown in Fig. 3. The total mass of the wing M_{tot} can then be calculated by defining the material density.

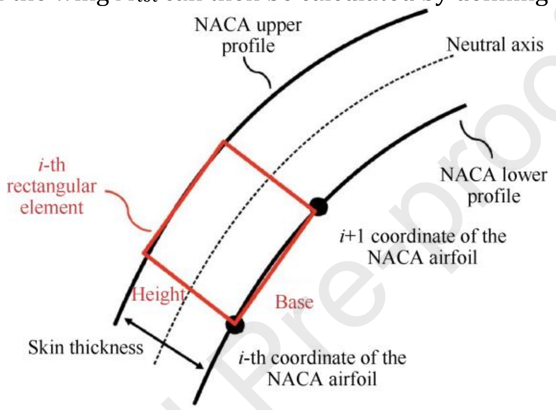

Fig. 2. Discretization of the skin cross-section.

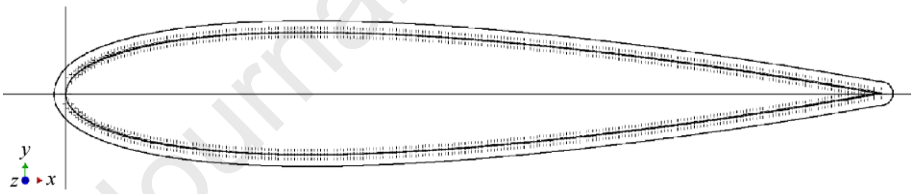

Fig. 3. Airfoil construction through NACA thickness function.

2.3. Dynamic analysis

The behavior of the equivalent system is described by Newton's equation of motion shown in Eq. (7)

$$F - kx = \left(\frac{K_M}{K_L}\right)Ma \quad (7)$$

where x is the displacement and a the acceleration of the SDOF system. The blast load acting on the structure is represented by F, and it is modeled with a linearly decaying triangular profile in time described by overpressure peak P_{r} and duration t_{pos}. The mass of the equivalent structure is M, and it considers all the relevant structural elements of the wing, as mentioned above. The stiffness of the equivalent structure is represented by k, whose value for cantilever beams subjected to uniformly distributed loads is tabulated in Ref. [16]. Stiffness k is influenced by the inertia of the wing, J_{tot}, and by Young's modulus E. The mass factor K_M and load factor K_L are two transformation factors that allow obtaining the equivalent lumped mass and the equivalent concentrated load of the SDOF system, respectively. These factors are evaluated as in Eqs. (8) and (9)

$$K_M = \frac{M_E}{M} \quad (8)$$

$$K_L = \frac{F_E}{F} \quad (9)$$

where M_E and F_E are the mass and the force of the equivalent beam element, and are evaluated by integrating the shape function $\phi(x)$ of such element along its length L, as in Eqs. (10) and (11).

$$M_E = \int_0^L m(x)\phi^2(x)\mathrm{d}x \tag{10}$$

$$F_E = \int_0^L p(x)\phi(x)\mathrm{d}x \tag{11}$$

At each time instant t, the equivalent system deflection $x(t)$ is evaluated through the predictor-corrector method [16]. At the first time instant, the initial acceleration a_0 is found through Eq. (7) by imposing the initial conditions $v_0=x_0=0$. Then, at each step of the analysis, the updated value of the deflection is evaluated based on the values of velocity and acceleration calculated at the previous step (prediction-correction). The procedure terminates either when $x(t)$ exceeds the value of maximum allowable deflection x_u, meaning that the plasticity condition has been reached, or when the time of the analysis exceeds a certain threshold, meaning that no plasticization has occurred. The maximum allowable deflection x_u is estimated through Eq. (12) [16]

$$x_u = \frac{2M_u}{k \cdot L^2} \tag{12}$$

where M_u, as defined in Ref. [16], is the ultimate moment capacity of the structure, accounting for the plasticization criterion of the wing. As shown in Eq. (13), M_u is a function of the yield strength σ_y and Young's modulus E.

$$M_u = f_{\mathrm{ds}} \cdot Z \tag{13}$$

where f_{ds} is the dynamic design stress of the material and Z is the plastic section modulus, which is calculated through Eqs. (14) and (15)

$$f_{\mathrm{ds}} = DIF \cdot a \cdot \sigma_y \tag{14}$$

$$Z = 1.5 \cdot S \tag{15}$$

where DIF and a are coefficients that take into account the dynamic response of the structure when it is subjected to dynamic loadings. S is the static section modulus. It must be noted that Eqs. (13)–(15) are valid for materials with values of the ductility ratio μ ranging between 3 and 10 [16, 23]. The ductility ratio is defined as the ratio between the maximum deflection X_m and the equivalent elastic one X_E.

2.4. Vulnerability assessment

The modules described above have been integrated into the in-house vulnerability software already presented by the authors in Refs. [2, 3]. The software can now deal with impacting projectiles in single-hit and multi-hit scenarios, fragments from detonating threats, and blast waves. The description of the whole software is out of the scope of this work. The interested reader is referred to Refs. [2, 3] for additional details. Hence, only the vulnerability assessment to blast waves is described below. A hemispherical grid, namely the detonation grid, is constructed around the target platform model, and detonation points are defined within such a grid. Each detonation point represents the position from which the detonating object goes off. That is, each detonation point generates a blast wave that the software will consider in the assessment. The hemispherical grid is centered on the geometric center of the platform, and its radius identifies the detonation distance between the threat and the target. To provide more informative results, the software allows for defining multiple detonation distances, within a single analysis, as shown in Fig. 4 for five detonation distances. The distances are defined as the length of the line connecting the center of the target with the detonation point. Each detonation point is considered independently during the vulnerability assessment, meaning that one blast wave at a time impacts the target platform. The description of how the hemispherical grids are constructed is reported in Ref. [2], and it is not written here in the interest of brevity. Fig. 5 shows the 2D projection of a representative hemispherical grid. In this case, the detonation points are identified by black dots, and numbers identify the outcome of the vulnerability assessment at each considered point (1: damaged platform, 0: undamaged platform).

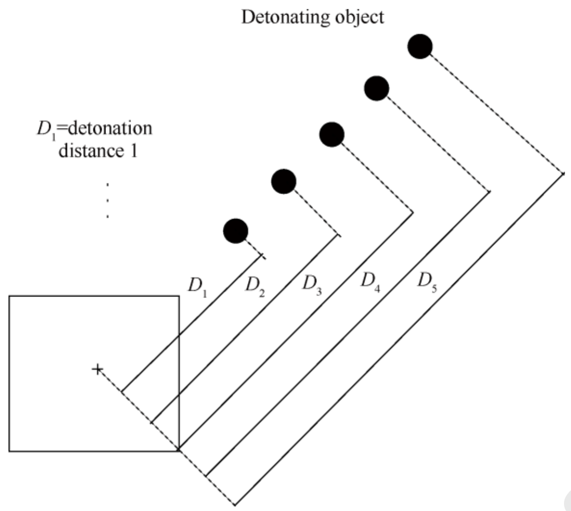

Fig. 4. Detonation distances considered in the assessment.

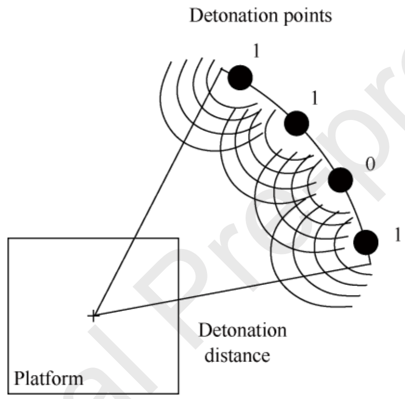

Fig. 5. Two-dimensional projection of a representative hemispherical grid around the platform.

According to what has already been mentioned above in subsection 2.2, the geometric module of the software determines the structural characteristics of the target platform, the wing in this case, necessary to evaluate its deflection. Subsequently, considering a detonation distance, the software calculates the characteristics of the pressure waves originating from each detonation point composing the grid at the analyzed distance. These characteristics are derived according to subsection 2.1. Then, the dynamic module described in subsection 2.3 is used to evaluate the deflection of the equivalent structure and, consequently, assess its operability. This evaluation is performed for each detonation point within the considered hemispherical grid, and subsequently repeated for each detonation distance.

During each vulnerability assessment, the blast-loaded structure is considered inoperative if it undergoes a larger deflection than the allowable deflection. In such case, the software assigns a kill probability of 1 to the detonation point, while 0 is assigned otherwise, as shown in Fig. 5. Then, the average of the kill probabilities of all detonation points within the same hemispherical grid is computed. This value is the vulnerability of the platform at the detonation distance that corresponds to the considered hemispherical grid.

3. Case Study

This section first goes through the validation of the dynamic module described in subsection 2.3 by comparing the analytical predictions for blast-loaded Representative beams with the results of finite element simulations run in the Abaqus©/CAE environment. Then, a wing of an aerial platform is considered to show the capabilities of the proposed framework for vulnerability assessment to blast loading.

3.1. Dynamic module validation against blast-loaded beams

The dynamic module described in subsection 2.3 was validated against six beam configurations obtained by combining

- Three different beam cross-sections;
- Two boundary conditions: cantilever beam and beam clamped at both ends.

Double-clamped beams were expected to undergo a fully elastic phase, followed by an elastic-plastic phase during which plastic hinges appear, and by a fully plastic phase during which the midsection undergoes plasticity. Instead, cantilever beams were anticipated to only present a fully elastic phase followed by a fully plastic phase, which happens as soon as the clamped section undergoes plasticity. All the structures are 500 mm long, have a rectangular cross-section, and are made of Steel 4340, whose physical properties are reported in Table 1. The six structural configurations considered for validation are summarized in Table 2. Several loading conditions were considered for each structural configuration, as shown in Tables 3 and 4 for double-clamped and cantilever beams, respectively.

Table 1
Physical properties of Steel 4340 [24].

Property	Value	Units
Density	7800	$kg \cdot m^{-3}$
Young's modulus	210	GPa
Poisson's Ratio	0.33	-

Table 2
Beam configurations considered for validating the dynamic module.

Boundary condition	Cross-section/mm^2
Double-clamped beam	20×10
Double-clamped beam	20×20
Double-clamped beam	20×50
Cantilever beam	20×10
Cantilever beam	20×20
Cantilever beam	20×50

Table 3
Loads considered for double-clamped beams.

Section	20 mm×10 mm	20 mm×20 mm	20 mm×50 mm
Loads/Pa	1.0×10^6	1.0×10^6	1.0×10^7
	2.0×10^6	5.0×10^6	3.0×10^7
	4.0×10^6	7.0×10^6	4.5×10^7
	7.0×10^6	1.0×10^7	7.0×10^7
	1.0×10^6	1.5×10^7	8.0×10^7
	1.2×10^6	2.0×10^7	1.0×10^8

Table 4
Loads considered for cantilever beams.

Section	20 mm×10 mm	20 mm×20 mm	20 mm×50 mm
Loads/Pa	1.0×10^5	1.0×10^5	1.0×10^6
	2.0×10^5	5.0×10^5	3.0×10^6
	4.0×10^5	7.0×10^5	5.0×10^6
	7.0×10^5	1.0×10^6	7.0×10^6
	1.0×10^6	1.5×10^6	1.0×10^7
	1.2×10^6	2.0×10^6	1.3×10^7
	1.5×10^6	2.5	1.6
	2.0×10^6	3.0	1.8
	3.0×10^6	5.5	2.0

The analytical deflections computed by the proposed approach were compared to those from numerical simulations. Beams were numerically modeled through 2D wires with a fixed length of 500 mm. The material parameters for the Johnson-Cook constitutive law are reported in Table 5.

Table 5
Steel 4340 Johnson-Cook parameters [24].

Property	Value	
Strain rate correlation	-	First-order
Initial yield stress	792	MPa
Hardening constant	510	MPa
Hardening exponent	0.26	-
Strain rate constant	0.014	-
Thermal softening exponent	1.03	-
Melting temperature	1793	K
Reference strain rate	1	-

The load in the numerical simulations was modeled as a line load with a triangular distribution in time. Two representative configurations are shown in Figs. 6 and 7.

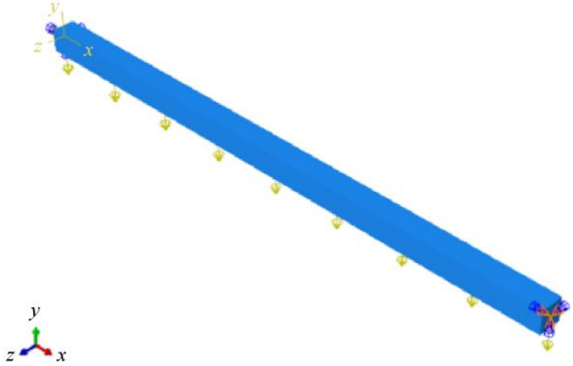

Fig. 6. Double-clamped beam with 20 mm×20 mm rectangular section, with line load applied.

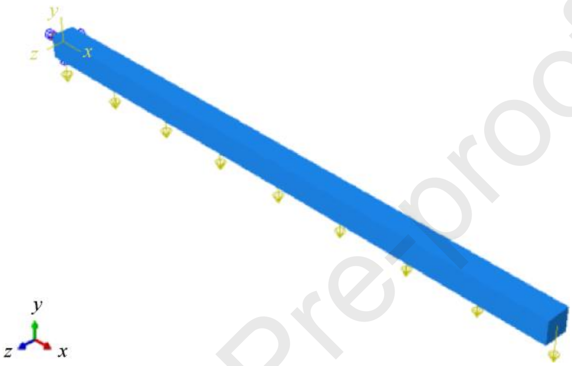

Fig. 7. Cantilever beam with20 mm×20 mm rectangular section, with line load applied.

The results for the double-clamped beams are shown in Fig. 8, where the predicted deflection at the midpoint of the beams is shown.

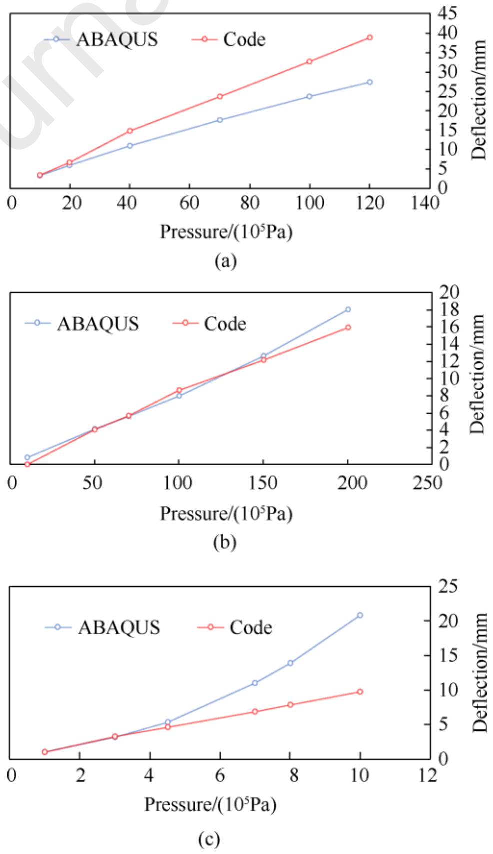

Fig. 8. Results of the deflection module and of the numerical simulations for double-clamped beams.

It turned out that the beam's slenderness influenced the predictions. That is, the numerically predicted deflection for beams with high slenderness was lower than that predicted by the deflection module, while the opposite occurred for the beam with cross-section 20 mm×50 mm. Moreover, evidence was brought that the proposed method adhered to the numerical results when the load was not enough to induce plasticity (first two loads reported in Table 3.

The results for cantilever beams are shown in Fig. 9. In this case, the predictions of the proposed method adhered to the numerical simulations for all configurations and load cases.

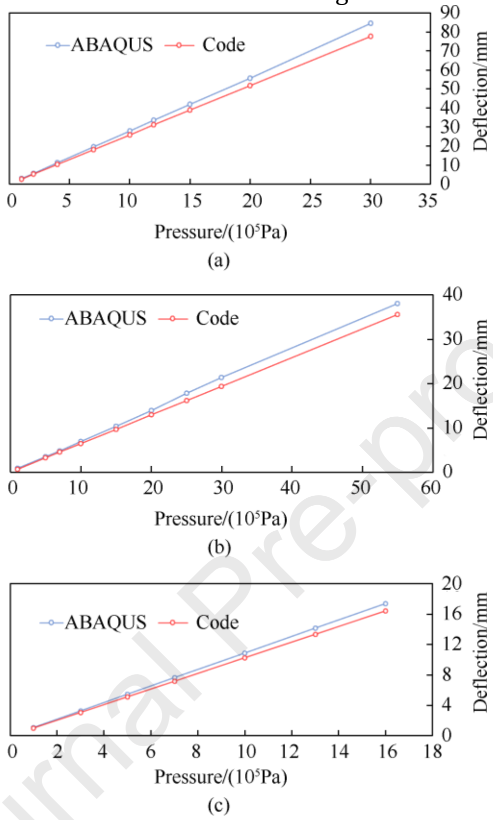

Fig. 9. Results of the deflection module and of the numerical simulations for cantilever beams.

3.2. Dynamic module validation against a representative blast-loaded wing

The structure considered in this work is based on the wing reported in Ref. [25], since detailed information is provided in the article. The wing, which was designed without taking into account any blast load alleviation solution, consists of (i) a box-shaped spar with a hollow rectangular cross-section, web thickness of 3.175 mm, and flange thickness of 9.525 mm, (ii) 9 ribs with thickness 1.6 mm, and (iii) the skin wrapping all the structural components mentioned above. The spar, with a hollow rectangular section, has the dimensions reported in Table 6, corresponding to the geometry shown in Fig. 10. Only half of the wing was modeled due to the symmetry of the aircraft.

Table 6
Spar dimensions [25].

Dimensions	Values/m
Length	4
B	0.15
b	0.144
H	0.1
h	0.08

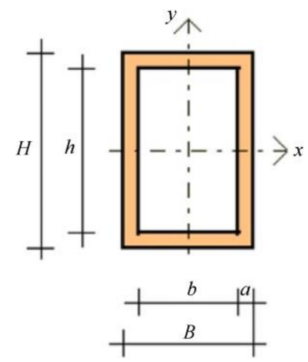

Fig. 10. Cross-section of the spar.

The wing was simplified as an equivalent beam, and the method implemented into the dynamic module was used for predicting the wing deflection due to blast loading. the results were then compared to expected values computed through numerical simulations.

The wing was made of Aluminum 7075T6, whose physical properties are reported in Table 7.

Table 7
Physical properties of Aluminum 7075T6.

Property	Value	Units
Density	2810.01	$kg \cdot m^{-3}$
Young's modulus	68.947	GPa
Poisson's Ratio	0.33	-
Yield strength	441	Mpa
Ultimate tensile strength	517	Mpa

In the numerical models, the material behavior was described through the Johnson-Cook model using the parameters reported in Table 8.

Table 8
Johnson-Cook parameters for Aluminum 7075T6 Ref. [26].

Property	Value	
Strain rate correlation	-	First-order
Initial yield stress	546	MPa
Hardening constant	678	MPa
Hardening exponent	0.71	-
Strain rate constant	0.024	-
Thermal softening exponent	1.56	-
Melting temperature	893	K
Reference strain rate	0.005	-

The structural components of the wing, i.e., ribs, spars, and skin, were modeled using 2D shell elements with reduced integration: a triangular mesh with S3R elements was used for the ribs, while linear four-node shell elements (S4R) for the spars and the skin. The global mesh size was 12 mm for the ribs, and 20 mm for the spars and the skin. The element size was defined after a convergence analysis, which is not reported here for conciseness. The wing was clamped at the root by fixing all degrees of freedom of (i) the rib located at the wing root, and (ii) the spar edge at the wing root. The half-wing assembly and the boundary conditions are shown in Fig. 11.

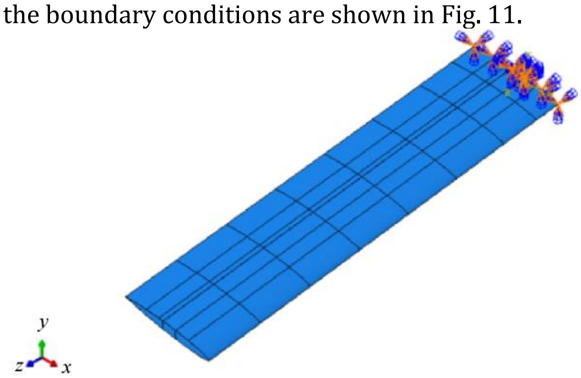

Fig. 11. Half-wing assembly.

The blast load was applied in the numerical models by exploiting the *Conwep* module in Abaqus©/CAE [27], which computes the overpressure profile and applies it to the structure. The only required input parameters for computing the blast load were the detonation position and the TNT equivalent charge. Several detonation positions and explosive charges were considered, and the maximum deflection of the wing tip was extracted for each load case. Moreover, the plastic deformation of the structural elements was also monitored.

First, the proposed approach was validated by comparing the overpressure profile parameters against those determined by the *Conwep* method. Two parameters were considered: the arrival time of the pressure wave at the wing, and the reflected overpressure value. For validation, a simulation involving a charge of 10 kg of TNT detonating 20 m from the wing surface along the y direction was considered. The numerical maximum reflected overpressure obtained was 22.94 kPa (Fig. 12), and the arrival time was 44.55 ms. The method described in subsection 2.1 predicted similar values. That is, a maximum reflected pressure of 25.02 kPa, and an arrival time of 40.29 ms were predicted by the proposed approach. The results are summarized in Table 9.

Table 9
Comparison of the blast load parameters obtained from Abaqus© and from the proposed approach.

Parameters	Numerics	Proposed approach	Difference/%
Pressure/kPa	22.94	25.02	-8.31
Time of arrival/ms	44.55	40.29	10.57

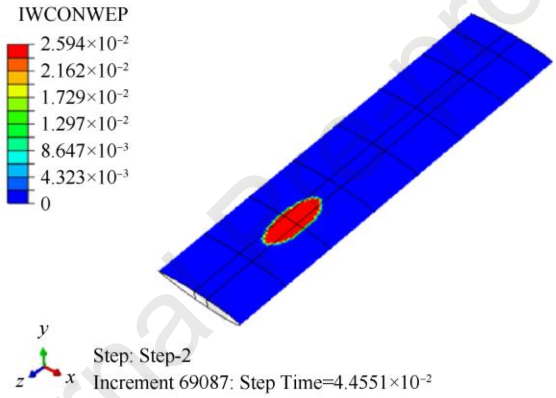

Fig. 12. Reflected overpressure predicted by Abaqus©.

After validation, several simulations were carried out by changing the explosive charge mass. That is, charges of 5 kg, 10 kg, and 30 kg at 20 m from the wing surface were considered. The tip deflections computed through the proposed approach and in the numerical simulations are compared in Table 10.

Table 10
Comparison of the tip deflection obtained by the proposed approach and through numerical simulations.

Charge/kg	Numerics/mm	Proposed approach/mm	Difference/%
5	129	126	-2.38
10	215	203	5.91
30	489	441	10.88

The detonation point was also moved along the wing span to identify any influence on the results. However, the deflection at the wing tip did not significantly change when moving the detonation point, as shown in Table 11 for a charge of 5 kg detonating at a vertical distance (*y* direction in Fig. 12) of 10 m from the wing, and considering five positions along the half-wing span. The difference between the maximum deflection, which happened when the charge detonated above the root of the wing, and the minimum one was 7 mm, which was considered negligible compared to the predicted deflection.

Table 11
Numerical deflection at the wing tip at different detonation positions along the half-wing span. Distance refers to the distance from the wing root along the *z*-axis.

Distance/mm	4000	3000	2000	1000	0
Deflection/mm	229	230	232	228	235

Based on such results, the dynamic module was validated by considering all the detonation points at a fixed position along the span of the half-wing, i.e. 3000 mm. Thus, only the detonation distance along the y direction and the charge mass were varied. Similarly to the assumption made for the deflection module, in the numerical simulations, the wing was considered no longer operative when the spar underwent plasticity. The results of a representative simulation involving a 10 kg charge detonating at 5 m distance from the wing are shown in Fig. 13. In such a load case, the wing underwent plasticity and was considered no longer operative.

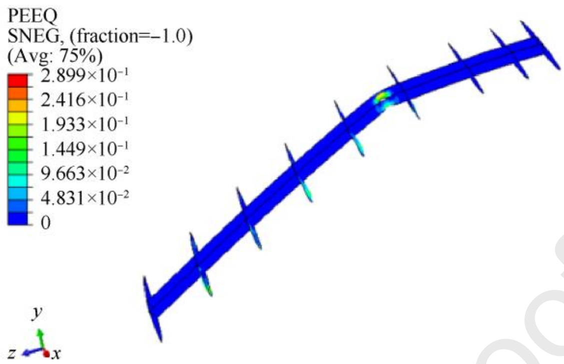

Fig. 13. Results of the numerical simulation with a charge of 10 kg detonating at 5 m distance. The skin was removed from the view to better show the spar and the ribs.

The results obtained from the numerical simulations and those provided by the proposed approach are shown in Table 12. The results bring evidence that the proposed approach adhered to the observations provided by the numerical simulations.

Table 12
Results of the validation analysis.

Detonation dist./m	Mass/kg	Numerics	Proposed approach
5	5	Inoperative	Inoperative
	10	Inoperative	Inoperative
	30	Inoperative	Inoperative
10	5	Operative	Operative
	10	Operative	Operative
	30	Inoperative	Inoperative
20	5	Operative	Operative
	10	Operative	Operative
	30	Operative	Operative

3.3. Case study vulnerability assessment

The proposed method for assessing the vulnerability of blast-loaded structures was implemented into the in-house vulnerability assessment presented by the authors in Refs. [2, 3]. The software was demonstrated by means of a case study involving the half-wing already described in subsection 3.2 as the target. The process consists of constructing a hemispherical grid around the target platform. Detonation points are then defined within this grid to represent various possible explosion origins. Each detonation point generates a blast wave, with the software assessing the effect of each blast wave independently on the target platform.

The grid's radius indicates the distance between the detonation points and the platform, allowing for the analysis of multiple detonation distances within a single assessment. For each distance, the geometric module of the software first evaluates the structural characteristics of the platform, which are crucial for determining the deflection caused by the blast waves. Using this information, the software calculates the pressure wave characteristics from each detonation point, as described in subsection 2.1. The dynamic module (subsection 2.3) then assesses the wing's deflection and determines its operability under blast loading.

The software classifies the structure as inoperative if the deflection exceeds the allowable limit, assigning a kill probability of 1 to that detonation point, and 0 otherwise. Finally, it calculates the average kill probability for all detonation points within a hemispherical grid, representing the platform's vulnerability at that specific detonation distance. This process is repeated for each distance to provide a comprehensive vulnerability assessment of the target platform under different blast scenarios. The input variables used for this specific case study are summarized in Table 13.

Table 13

Input variables of the specific case study.

Input variable	Value
Range of detonation distances	7–10 m
Number of detonation distances	4–10 m
Number of detonation points	197
Detonation height (sea level)	500 m
Warhead case length	381 mm
Warhead case diameter	177.8 mm
Warhead case thickness	10.16 mm
Explosive's energy per unit mass	3780 kJ·kg^{-1}
Explosive's density	1560 kJ·kg^{-1}

The assessment results are shown in Fig. 14 in terms of platform vulnerability versus detonation distance. The vulnerability at each considered detonation distance was computed as the average probability that the wing would be made inoperative by an object detonating at that detonation distance. Such probabilities were computed by averaging the vulnerability at all points within the same hemispherical surface. Four curves are shown, each one corresponding to a different discretization of the detonation distance range. The computational cost of the simulations is reported in the legend. It turns out that the computational cost linearly depends on the number of detonation distances considered within the range. Notably, the overall trend in the results is unaffected by the discretization, with the vulnerability curves exhibiting similar behavior across all cases.

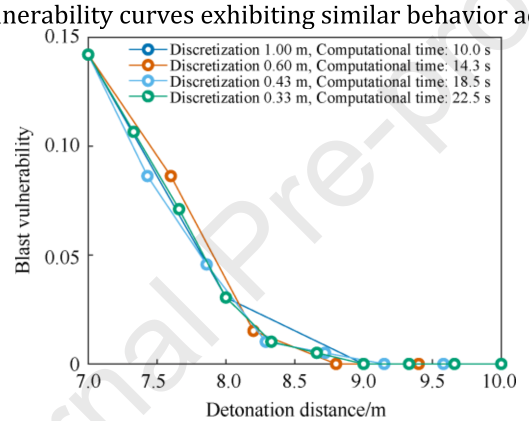

Fig. 14. Vulnerability values for each detonation distance.

Specifically, vulnerability decreased as the distance between the detonation point and the center of mass of the platform increased. This behavior is intuitive and adheres to the physics of the problem. In fact, the larger the detonation distance, the less critical the pressure time-history exerted on the structure. Specifically, vulnerability values ranged from 0% to 14%. The vulnerability values are reported in Table 14 for the curve with six detonation distances within the user-defined range.

Table 14

Vulnerability of the blast-loaded half-wing.

Detonation distance/m	Vulnerability/%
7.0	14.2
7.6	8.6
8.2	1.5
8.8	0.0
9.4	0.0
10.0	0.0

4. Conclusions

Considering vulnerability as a parameter in platform design, of any type, has become increasingly important in recent years. The results of these analyses can be taken into account during the preliminary conceptualization phase of the prototype as well as when the platform is already operational, for instance, if any measures are needed to reduce the platform's probability of becoming inoperative. In this context, this work aims to develop a module that enhances software designed and developed for vulnerability calculation. Specifically, this module can now calculate vulnerability by considering a shock wave impacting the structure as a threat. The module can analytically assess the resistance of the impacted structure without the need for finite element analysis, and subsequently evaluate the probability of the structure becoming inoperative.

Initially, the paper introduces the problem and presents the theoretical principles that enabled the assessment of loads acting on structures undergoing vulnerability analysis. A constant-section wing serves as a case study to illustrate the methodologies used to model its geometry correctly, analytically evaluate its dynamic properties, and ultimately calculate its vulnerability.

The described methodologies have been validated for the analyzed case study, with the conducted simulations reported. Specifically, the paper first presents simulations regarding the behavior of a beam impacted by blast loads. The beam, with a rectangular cross-section, is analyzed considering various dimensions and two different boundary conditions: fixed at one end and fixed at both ends. These simulations were conducted to validate the implemented SDOF approach for calculating accelerations, velocities, and displacements of the structure under shock wave stresses.

This work also validated the methodology used to evaluate parameters related to the shock wave and the software's capability to accurately predict the failure of the structure. Simulations were performed using the CONWEP module of the ABAQUS software on a wing model composed of a rectangular spar, ribs, and skin.

Finally, the results obtained from applying the software to the analyzed case study are reported, particularly the vulnerability values obtained at various detonation distances. For the analyzed case study, the implemented software can converge to the presented results within a few seconds, providing a significant update to the built-in software developed for vulnerability calculation. One of the key advantages of the developed tool lies in its computational efficiency. In fact, by using an approach based on the analytical calculation of the deflection and the vulnerability of the structure, finite element analyses (FEA) conducted for each detonation point are no longer required. A traditional FE approach would require conducting separate simulations for each detonation point and assessing if the displacement of the wing exceeds its structural limit to determine failure. Such an approach would require several hours to conduct a comprehensive vulnerability analysis due to the extensive computational requirements. In contrast, the developed tool computes the structure's vulnerability in just a few seconds, significantly reducing computation time while maintaining a reasonable level of accuracy. This makes the method particularly suited for rapid assessments and scenarios requiring numerous iterations or probabilistic analyses. Given the nature of the methodology used, the results obtained by considering shock waves impacting the structure are probability values that should not be interpreted as absolute probabilities of the structure becoming inoperative, but rather as comparative tools when multiple analyses on different structures are conducted.

Moreover, the limitations of the analytical models should be considered. The models are based on assumptions that make them efficient for simplified geometries. That is, their accuracy diminishes when applied to complex structures due to the inability to fully capture intricate geometric details, stress concentrations, and non-linear material behaviors that may arise in real-world scenarios. However, the primary aim of the analytical model considered in this work is to offer a balance between computational efficiency and accuracy, so to make the framework suitable for preliminary design phases or probabilistic assessments.

Evaluating vulnerability to shock waves represents an innovative element in this field, especially in the context of a developed algorithm using analytical theoretical models without necessarily using finite element simulations. The results obtained from vulnerability analyses can generate useful information at various stages of design, leading to precise design choices or corrective solutions that increase the probability of the platform surviving this type of scenario.

Future work may involve implementing deep learning algorithms to construct more accurate surrogate models for more complex simulations of structures subjected to extreme loading conditions, such as shock waves. These surrogate models could allow for faster and more precise predictions of structural behavior under a wide range of blast scenarios, bridging the gap between fully analytical models and detailed numerical simulations.

Additionally, future research may explore extending the tool's capabilities to address a broader variety of loading conditions, such as combined blast and impact scenarios or highly asymmetric load distributions. Moreover, once vulnerability values are obtained, they can be contextualized to drive the design process more effectively. This could involve integrating the tool into an iterative design optimization loop, where different structural layouts or material choices can be evaluated to mitigate the effects of shock waves on the structure, thereby reducing the probability of failure. Extending the current tool for use in real-time decision-making, for example in operational risk assessments, is another potential direction, providing immediate assessments to support strategic decisions in critical scenarios.

Declaration of competing interests

The authors declare that they have no known competing financial interests or personal relationships that could have appeared to influence the work reported in this paper.

Reference

[1] R. E. Ball, The Fundamentals of Aircraft Combat Survivability: Analysis and Design, 2nd Edition, American Institute of Aeronautics and Astronautics, 2003. doi:10.2514/4.862519.

[2] S. Annunziata, L. Lomazzi, M. Giglio, A. Manes, Topological optimization of ballistic protective st ructures through genetic algorithms in a vulnerability-driven environment, Defence Technolog y (2024). doi:https://doi.org/10.1016/j.dt.2024.05.011.

[3] L. Lomazzi, F. Cadini, M. Giglio, A. Manes, Vulnerability assessment to projectiles: Approach defi nition and application to helicopter platforms, Defence Technology 18 (9) (2022) 1523–1537.

[4] J. M. Vice, Survivability/vulnerability information analysis center (surviac) - a tool for the aircr aft survivability community, Journal of Aircraft 24 (1987) 511–515. doi:10.2514/3.45468.

[5] U. A. C. of Engineers, Unified facilities criteria (ufc): Structures to resist the effects of accidental explosions (2005). URL http://dod.wbdg.org/.

[6] P. Castelletti, S. Sangaletti, Vulnerability and survivability assessment of a new helicopter (201 8).

[7] J. N. Robert Edwin, A case study of a combat aircraft's single hit vulnerability (1986). URL https: //calhoun.nps.edu/handle/10945/21703

[8] E. D. Aitken, S. L. Jones, A. W. Fean, A Guide to FASTGEN Target Geometric Mode, Defense Techn ical Information Centre, 1993.

[9] Y. Pei, W. Wang, L. Li, Ranking the vulnerable components of aircraft by considering performan ce degradations, Journal of Aircraft 53 (2016) 1400–1410. doi:10.2514/1.C033683/ASSET/IM AGES/LARGE/ FIGURE7.JPEG. URL https://arc.aiaa.org/doi/10.2514/1.C033683

[10] Y. Pei, T. Cheng, Importance measure method for ranking the aircraft component vulnerability, Journal of Aircraft 51 (2014) 273–279. doi: 10.2514/1.C032334/ASSET/IMAGES/LARGE/FIGU RE3.JPEG. URL https://arc.aiaa.org/doi/10.2514/1.C032334

[11] P. Yang, S. Bifeng, H. Qing, Shot line geometric description method for aircraft vulnerability calc ulation, Chinese Journal of Aeronautics 22 (2009) 498–504. doi:10.1016/S1000-9361(08)6013 2-6.

[12] Y. Pei, B. F. Song, Solving the combinatorial explosion problem when calculating the multiple-hi t vulnerability of aircraft, https://doi.org/10.2514/1.18623 43 (2012) 1190–1194. doi:10.251 4/1.18623. URL https://arc.aiaa.org/doi/10.2514/1.18623

[13] H. E. Konokman, A. Kayran, M. Kaya, Analysis of aircraft survivability against fragmenting warh ead threat, American Institute of Aeronautics and Astronautics, 2014. doi:10.2514/6.2014-035 5.

[14] H. E. Konokman, A. Kayran, M. Kaya, Aircraft vulnerability assessment against fragmentation w arhead, Aerospace Science and Technology 67 (2017) 215–227. doi:https://doi.org/10.1016/j. ast.2017.04.005. URL https://www.sciencedirect.com/science/article/pii/S12709638173059 16

[15] L. Han, Q. Han, Y. X. Ge, X. Q. Sang, Vulnerability assessment of combat aircraft to blast loading, Proceedings of the Institution of Mechanical Engineers, Part G: Journal of Aerospace Engineerin g 233 (2019) 604–615. doi:10.1177/0954410017740162.

[16] U. A. C. of Engineers, Unified facilities criteria (ufc): Structures to resist the effects of accidental explosions (2005). URL http://dod.wbdg.org/.

[17] B. Hopkinson, British ordnance board minutes report 13565 (1915).

[18] K. J. Cranz, O. Eberhard, K. E. Becker, Lehrbuch der Ballistik, Vol. 2, Springer, 1926.

[19] S. Glasstone, P. J. Dolan, The effects of nuclear weapons (1977).

[20] L. Lomazzi, M. Giglio, A. Manes, Analysis of the blast wave – structure interface phenomenon in case of explosive events, IOP Conference Series: Materials Science and Engineering 1038 (2021) 012083. doi:10.1088/1757-899x/1038/1/012083.

[21] Ullah, F. Ahmad, H. W. Jang, S. W. Kim, J. W. Hong, Review of analytical and empirical estimation s for incident blast pressure, KSCE Journal of Civil Engineering 21 (2017) 2211–2225. doi: 10.1 007/s12205-016-1386-4.

[22] M. Drela, Course of unified engineering - lab 11 (2007). URL https://web.mit.edu/16.unified/w ww/archives%202007-2008/spring%20temps/psets/systems/beambend.pdf

[23] N. Jones, Structural Impact, Cambridge University Press, 2012.

[24] Z.-y. Wang, Y. Zhao, G.-w. Ma, Z.-g. He, A numerical study on the high-velocity impact behavior of pressure pipes, Journal of Zhejiang University-SCIENCE A 17 (6) (2016) 443–453.
[25] P. Bunyawanichakul, V. Sripawadkul, Design of a wing structure for a single turboprop normal category aircraft, International Journal of Aviation Science and Technology vm03 (2022) 45–57. doi:10.23890/ ijast.vm03is01.0105.
[26] A. Shah, R. Khan, S. S. R. Koloor, M. Petru, S. Badshah, S. Ahmad, M. Amjad, Finite element analysis of the ballistic impact on auxetic sandwich composite human body armor, Materials 15 (6) (2022) 2064.
[27] F. Saifi, S. Anas, R. Tahzeeb, M. Shariq, M. Alam, Numerical investigation of blast loading effects on a thin-walled cylindrical steel storage tank, Materials Today: Proceedings (2024). doi:https://doi.org/10.1016/j.matpr.2024.04.001. URL https://www.sciencedirect.com/science/article/pii/ S2214785324001883

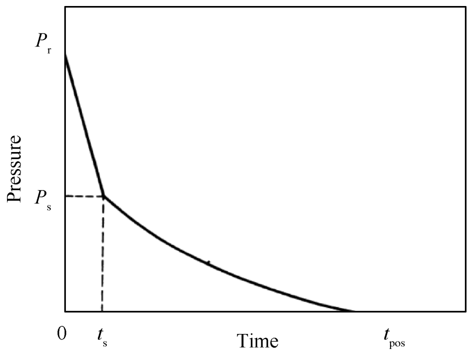

P_r
P_s
Pressure
0
t_s
Time
t_{pos}

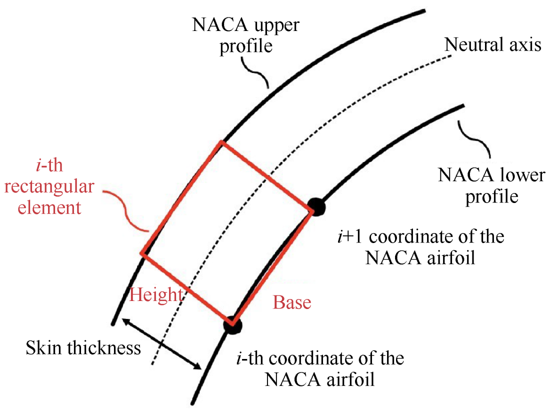
NACA upper
profile
Neutral axis
NACA lower
profile
i-th
rectangular
element
i+1 coordinate of the
NACA airfoil
Height
Base
Skin thickness
i-th coordinate of the
NACA airfoil

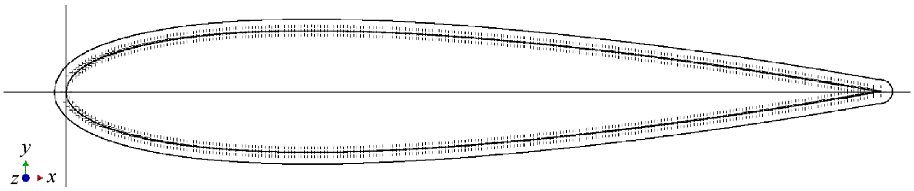
y
z
x

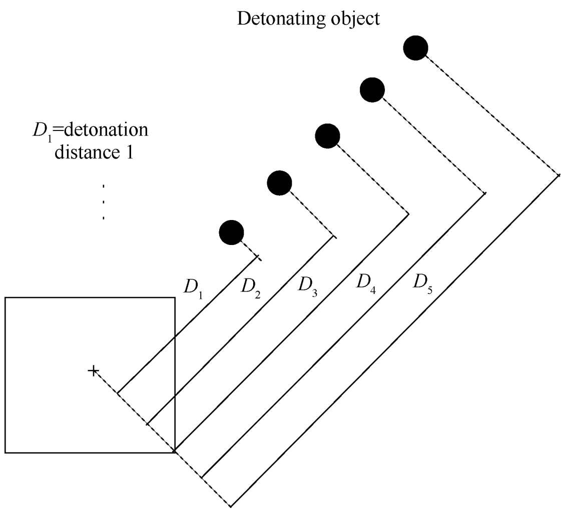
Detonating object
D_1=detonation distance 1
D_1
D_2
D_3
D_4
D_5

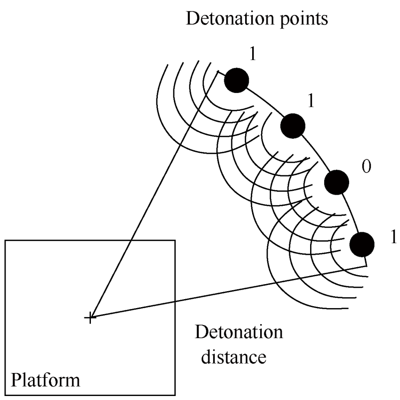
Detonation points
1
1
0
1
Platform
Detonation
distance

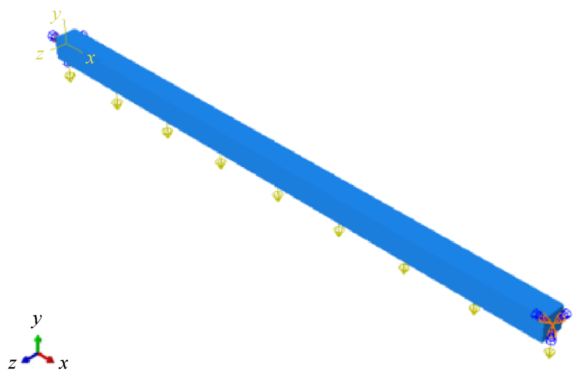
y
z
x
y
z
x

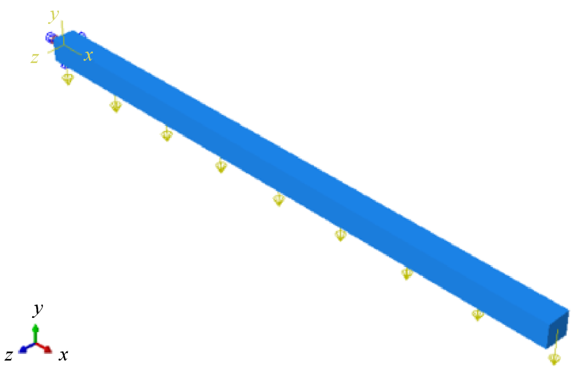

y
z
x
y
z
x

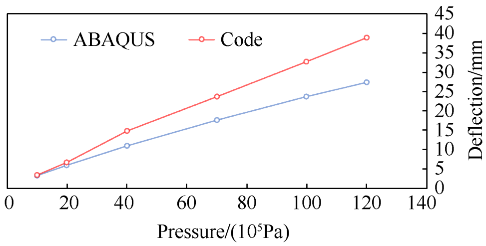
ABAQUS
Code
Deflection/mm
Pressure/(10⁵Pa)
0 20 40 60 80 100 120 140
0 5 10 15 20 25 30 35 40 45

(a)

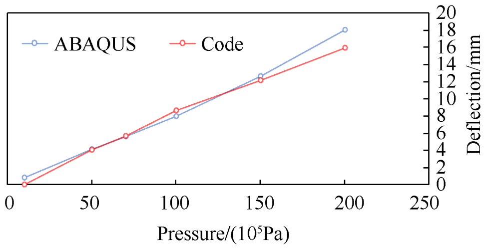
ABAQUS
Code
Deflection/mm
Pressure/(10⁵Pa)
0 50 100 150 200 250
0 2 4 6 8 10 12 14 16 18 20

(b)

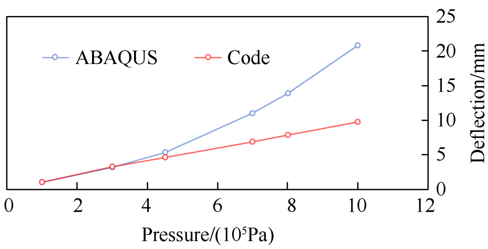
ABAQUS
Code
Deflection/mm
Pressure/(10⁵Pa)
0 2 4 6 8 10 12
0 5 10 15 20 25

(c)

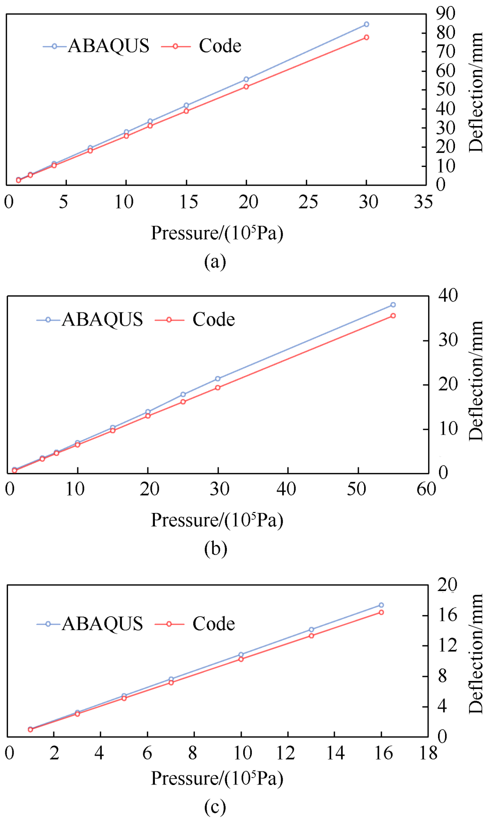
ABAQUS
Code
Deflection/mm
Pressure/(10⁵Pa)
(a)
ABAQUS
Code
Deflection/mm
Pressure/(10⁵Pa)
(b)
ABAQUS
Code
Deflection/mm
Pressure/(10⁵Pa)
(c)

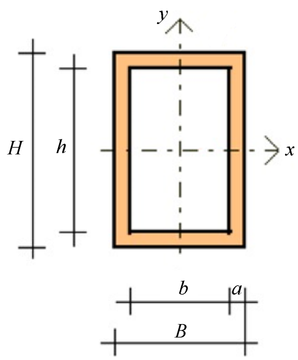
y
x
H
h
b
a
B

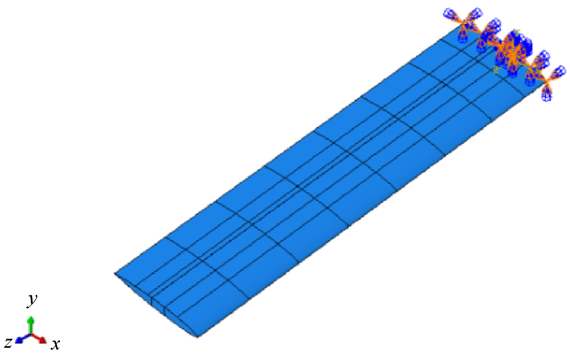
y
z
x

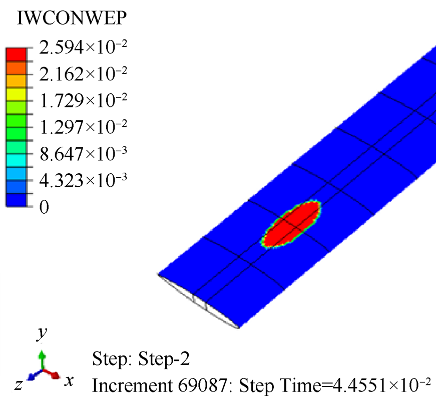
IWCONWEP
2.594×10⁻²
2.162×10⁻²
1.729×10⁻²
1.297×10⁻²
8.647×10⁻³
4.323×10⁻³
0
y
z
x
Step: Step-2
Increment 69087: Step Time=4.4551×10⁻²

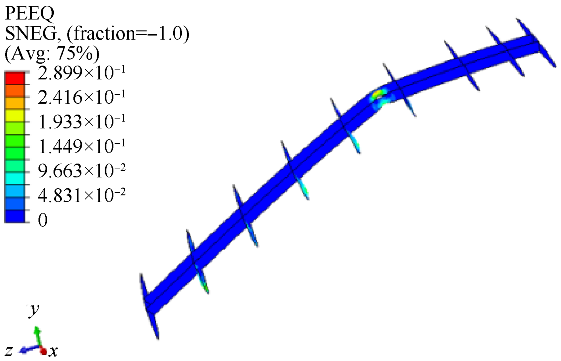
PEEQ
SNEG, (fraction=−1.0)
(Avg: 75%)
2.899×10⁻¹
2.416×10⁻¹
1.933×10⁻¹
1.449×10⁻¹
9.663×10⁻²
4.831×10⁻²
0
y
z
x

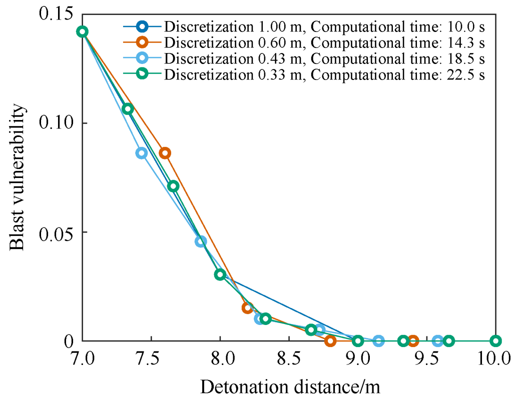
0.15
0.10
0.05
0
7.0
7.5
8.0
8.5
9.0
9.5
10.0
Blast vulnerability
Detonation distance/m
Discretization 1.00 m, Computational time: 10.0 s
Discretization 0.60 m, Computational time: 14.3 s
Discretization 0.43 m, Computational time: 18.5 s
Discretization 0.33 m, Computational time: 22.5 s

Declaration of interests

☒ The authors declare that they have no known competing financial interests or personal relationships that could have appeared to influence the work reported in this paper.

☐ The author is an Editorial Board Member/Editor-in-Chief/Associate Editor/Guest Editor for *[Journal name]* and was not involved in the editorial review or the decision to publish this article.

☐ The authors declare the following financial interests/personal relationships which may be considered as potential competing interests: